

# Comparison of frequency, linewidth, and output power in measurements of spin-transfer nanocontact oscillators

W. H. Rippard, M. R. Pufall, and S. E. Russek

*Electromagnetics Division, National Institute of Standards and Technology, Boulder, Colorado 80305, USA*

(Received 11 September 2006; published 13 December 2006)

We have measured the detailed dependence of the oscillation frequencies, linewidths, and output powers of spin-transfer nanocontact oscillators as functions of applied field strength, bias current, and angle of the applied magnetic field. For fields applied only moderately out of the plane of the film, the evolution of these properties is continuous. However, for fields applied more strongly out of plane they exhibit discontinuous evolution in both current and applied field. These discontinuities typically correlate with changes in the device resistance, changes in device output power, and a broadening of their spectral linewidths. However, away from these discontinuities, the oscillator output powers are larger and the linewidths narrower when compared to geometries having the fields applied at smaller angles. Our measurements suggest that the discontinuous evolution of the frequency with current and applied field results from an abrupt change in the precessional mode of the free layer.

DOI: [10.1103/PhysRevB.74.224409](https://doi.org/10.1103/PhysRevB.74.224409)

PACS number(s): 75.47.De, 85.75.-d

## I. INTRODUCTION

Since the initial predictions that a spin-polarized current can exert a torque on a nanoscale magnet,<sup>1,2</sup> much progress has been made in understanding the spin-transfer effect and its manifestations. A number of groups have successfully demonstrated both current-induced switching and steady-state magnetic precession in patterned magnetic nanostructures,<sup>3-9</sup> nanowires,<sup>10</sup> and nanocontacts,<sup>11-14</sup> as well as current-induced motion of domain walls.<sup>15</sup> Theoretical efforts to better understand these effects have included analytical approaches,<sup>16-23</sup> numerical single-domain modeling,<sup>24-26</sup> and more recently, micromagnetic simulations,<sup>27-29</sup> and a general qualitative agreement between experiment and theory regarding the most basic results has been achieved.<sup>30</sup>

However, there are also a number of discrepancies between the measured behaviors of the precessional dynamics in magnetic nanocontacts and the behaviors predicted by both micromagnetic and single-domain modeling. For instance, as we discuss below, measurements show much more complicated behavior in the evolution of the precessional frequency with current and field than have been predicted by single-domain simulations and spinwave-based theories. Furthermore, the precessional dynamics in the nanocontact devices are much more persistent and robust than have been predicted by micromagnetic modeling.<sup>29</sup> In this paper we describe the characteristics of the spectral output of spin-transfer nanocontact oscillators (STNO) in detail and point out some of the differences between the measured behaviors and those predicted by models. All presented data are from a single device. However, the qualitative features and general trends that we concentrate on here have been observed in all measured devices, independent of device size or material.

The device discussed here consists of a single, nominally 50-nm-diam electrical contact made to the top of a continuous  $10 \times 20 \mu\text{m}$  spin-valve mesa. The spin valve comprises Ta(3 nm)/Cu(15 nm)/Co<sub>90</sub>Fe<sub>10</sub>(20 nm)/Cu(4 nm)/Ni<sub>80</sub>Fe<sub>20</sub>(5 nm)/Au(3 nm). In this structure, precessional motion is

induced in the NiFe layer, and the CoFe layer acts as the “fixed” layer due to its larger thickness and saturation magnetization. The devices are dc current biased so that precessional motion of the free layer induces a microwave voltage across the device through the giant magnetoresistance (GMR) effect. The spectral characteristics of the device output are measured with a spectrum analyzer. All measurements discussed here were performed at room temperature.

## II. RESULTS AND DISCUSSION

In a previous publication,<sup>31</sup> we showed that the *average* oscillation frequencies and output powers of STNO devices mimic a large-angle version of ferromagnetic resonance (FMR), in accordance with single-domain simulations. Here, we give a much more detailed presentation of the evolution of the oscillation frequency with field and current and compare this with the evolution of the oscillator linewidth and output power. In Fig. 1, we show surface plots of the oscillator precessional frequencies as functions of both current and applied field for applied field angles  $\theta_H$  between  $50^\circ$  and  $85^\circ$  out of the film plane. The surface plots are formed by measuring the device output as the current  $I_{dc}$  is stepped in increments of 0.25 mA and the field in increments of either 19.9 kA/m (250 Oe) or 39.8 kA/m (500 Oe) and linearly interpolating between these positions. The center frequency, linewidth [full width at half-maximum (FWHM)], and output power are determined by Lorentzian fits to the device output. The data are plotted for both increasing and decreasing current sweeps. There is no measurable hysteresis in these scans, so the plots are symmetric about the highest current value, but including both scan directions in the plots tends to make slight variations in the surface more visually apparent. If there are no precessional oscillations present for a particular combination of current, field, and angle, the frequency is taken to be zero, resulting in the appearance of side walls on the surface plots when the precession begins.

At the lowest field angle ( $50^\circ$ ) the evolution of the precession frequency is approximately planar, with the fre-

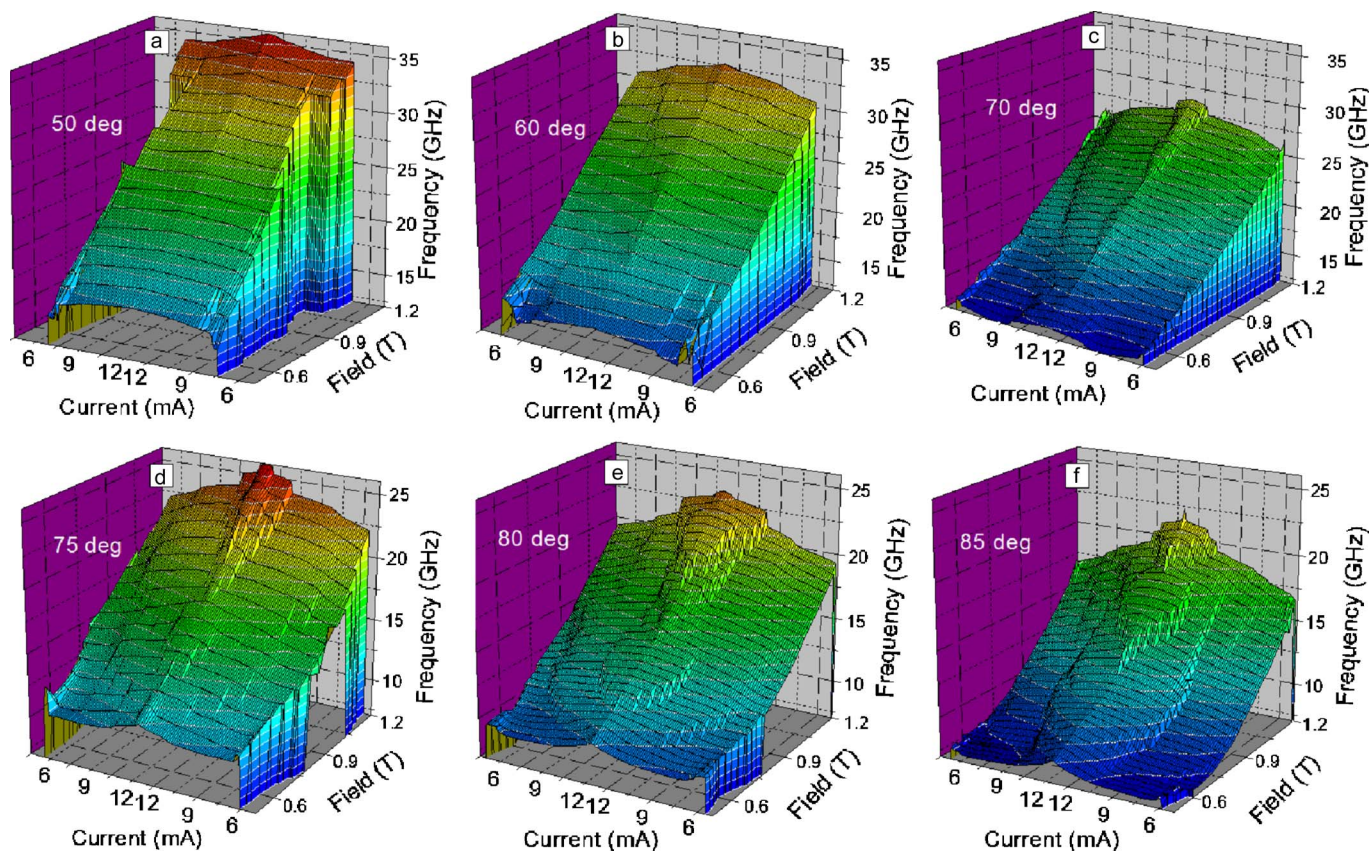


FIG. 1. (Color online) (a)–(f) Surfaces showing the oscillation frequency as functions of current and applied field for different applied field angles (noted on the plots). The frequency ranges for (A)–(C) are identical, as are the frequency ranges for (d)–(f). The color scale is linear and identical to the frequency range of each plot.

quency changing linearly with both field and current. The variation with current is roughly 0.5 GHz/mA, and the variation with field is about 28 GHz/T. As the field angle is increased to 60° the frequency surface remains qualitatively similar to the 50° surface, although there is more local variation in the surface gradient. As the angle of the applied field is further increased, the field tunability of the oscillations decreases while their current tunability increases. Note that the frequency range of the plots is the same for Figs. 1(a)–1(c) and changes for Figs. 1(d)–1(f). For instance, for  $\theta_H=80^\circ$  the variation with field is roughly 18 GHz/T, and the variation with current, although more variable, is roughly 1 GHz/mA. As discussed previously, the overall observed trend is in general agreement with single-domain simulations using the theoretical model of Slonczewski.

However, other features of the frequency surfaces have not been found in either single-domain simulations or micromagnetic simulations of nanocontact devices. For instance, as the applied field angle is increased to greater than about 70°, the frequency surface progressively takes on a different character, and there exist locations where the oscillation frequency evolves in a *discontinuous* manner with both current and field. These discontinuities can be seen at the highest currents and fields for the 70° surface and become more common at the higher applied field angles. The size of the frequency discontinuity varies with its location on the frequency surface and the applied field angle, but generally

ranges from a few hundred megahertz to several gigahertz and can be significant fractions (10–20%) of the oscillation frequency (see Fig. 1).

The positions of these discontinuities evolve relatively smoothly with field and current, forming frequency surfaces that have several plateaus separated by discontinuous steps. As seen by comparing Figs 1(d)–1(f), the escarpments formed by these discontinuities also change with  $\theta_H$  and generally become more prominent at the higher field angles. The exact locations (i.e., current and field values) of these discontinuities vary from device to device, perhaps resulting from variability in the material microstructure in the vicinities of the contacts or variation in the contact geometries themselves. However, their appearance at roughly these applied field angles, field strengths, and currents is consistent across the many tens of devices measured, as are the other qualitative features and trends we discuss below.

We describe these transitions as discontinuous at those locations because we typically find two precession frequencies in the acquired spectra: one corresponding to the higher frequency mesa and the second to the lower. One example of this is shown in Fig. 2. We interpret this as resulting from the existence of two distinct and stable precessional excitations with thermally activated switching between them. We have explicitly determined that the surface is discontinuous in both current and field. In Fig. 1 the discontinuities appear more clearly in current than field since the density of data in

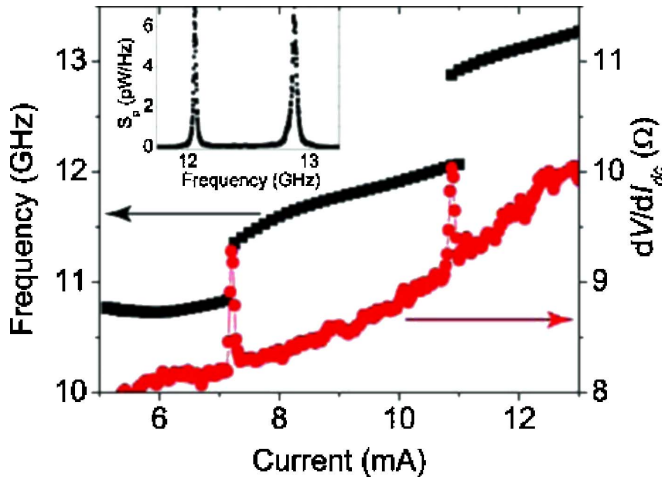


FIG. 2. (Color online) Plot showing the oscillation frequency and differential resistance vs  $I_{dc}$  for an applied field of 0.7 T and  $\theta_H=80^\circ$ . The data for increasing and decreasing current scans are plotted for both data sets. (Inset) Spectral power density showing two distinct frequencies as the discontinuity at  $I_{dc}=10.875$  mA.

the current direction is much greater. It is also clear that the surface must be discontinuous in both current and field since a curved ridge on a three-dimensional surface cannot be everywhere discontinuous in only one direction. Neither single-domain simulations nor micromagnetic models have predicted the existence of these discontinuous jumps.

In Fig. 2, we plot a representative differential resistance  $dV/dI_{dc}$  curve along with the excitation frequency for  $\theta_H=80^\circ$  and  $\mu_0H=0.7$  T. As seen in the figure, there are significant and reversible changes in the dc device resistance (peak in the differential resistance) at these discontinuities. This indicates that there is a significant change in the projection of the time-averaged orientation of the free layer onto the fixed layer, consistent with significant changes in the precessional motion of the free layer occurring at these locations. The change of the precessional mode could be, for instance, a significant change in the precessional angle of quasiumiform precession, or the precession changing from a quasiumiform mode to some other spatially nonuniform mode. We have found no correlation between the size of the changes in the dc resistance of the device and changes in the size of the frequency discontinuities.

The discontinuities could also result from the fixed layer undergoing a reorientation. However, we have measured devices that are identical to those discussed here but with a 75% thicker CoFe (35 nm) fixed layer. In both device sets we observe similar discontinuous frequency evolution at roughly the same currents, fields, and angles, indicating they do not result from a reorientation of the fixed layer. Furthermore, when a device is biased close to a discontinuity in the frequency surface it can be injection locked<sup>32</sup> to either the higher or lower frequency for fixed values of  $I_{dc}$  and  $|I_{ac}|$  and changing only the frequency of the injected ac current. Both of these results indicate that these discontinuities are associated with a change in the precessional motion of the free layer.

A number of experiments have established that at threshold the excited mode is well approximated by uniform pre-

cession of the magnetization, either in the vicinity of the contact area in the case of nanocontacts, or in the free-layer volume in the case of nanopillar devices.<sup>12,33</sup> Micromagnetic simulations have suggested that other precessional modes can be excited for currents significantly beyond threshold<sup>27,28</sup> and there is experimental evidence that such modes can be excited in nanopillar devices<sup>34</sup> where there are spatially varying demagnetization fields. However, the data shown in Fig. 1 are qualitatively different from those in Ref. 34. In the data presented there all modes have the same change in frequency with the applied field  $df/dH$  and hence remain distinct over at least a large range of applied field values. Here the case is quite different. When the frequency jump occurs, the plateau formed by the higher frequencies has a lower value of  $df/dH$  than the lower frequency plateau, so that they eventually merge at higher applied fields. This is explicitly seen for the larger angles of the applied field (e.g., Fig. 1(f) with  $\mu_0H=1.1$  T for  $I=9$  and 12 mA), but cannot be checked at lower field angles because of limitations on the applied field strength.

In Fig. 3(a) we show a surface plot of the linewidth  $\Delta f$  (FWHM) mapped onto the frequency surface for an applied field angle of  $80^\circ$  [Fig. 1(e)]. The linewidth varies by several orders of magnitude over the surface and is shown in a logarithmic color scale. Clear correlations exist between  $\Delta f$  and the frequency surface. For instance, when there is a discontinuity in the frequency there is a corresponding increase in the linewidth (although the amount of this increase varies with location). The linewidth similarly increases when there is a rapid, but continuous, change in the frequency. The locations of the discontinuities and large surface gradients in the frequency surface are highlighted in the plot of the differentiated frequency surface in Fig. 3(b) (discussed in more detail below). This behavior will occur in any tunable oscillator. Noise in a parameter that changes the oscillation frequency will also cause the oscillation linewidth to broaden. Here the sources of noise will include instrumentation noise as well as thermal noise, i.e., Johnson noise, shot noise, and thermal field noise. In order to quantitatively model the linewidth from a frequency surface the relative strengths of each of these contributions will need to be determined along with any other sources of linewidth broadening, such as inhomogeneous broadening.

Determining the relative strengths of each of the various noise contributions to the spectral linewidths is beyond the scope of this paper. Instead, we compare the measured linewidths to a simplified model that assumes that low-frequency instrumentation noise in the applied field and current are the dominant sources of linewidth broadening. The surface shown in Fig. 3(b) is calculated through

$$\Delta f = \left( \left( \frac{\partial f}{\partial H} \right)^2 (\Delta H)^2 + \left( \frac{\partial f}{\partial I_{dc}} \right)^2 (\Delta I_{dc})^2 \right)^{1/2}, \quad (1)$$

where  $\mu_0\Delta H=0.1$  mT is the measured field noise in an approximately 100 Hz bandwidth and  $\Delta I_{dc}=1$   $\mu$ A is the measured noise from the power supply in a 10 kHz bandwidth. The derivatives are calculated using a multipoint numerical differentiation of the frequency surface. For the  $\theta_H=80^\circ$  data, there is a general correlation between regions having

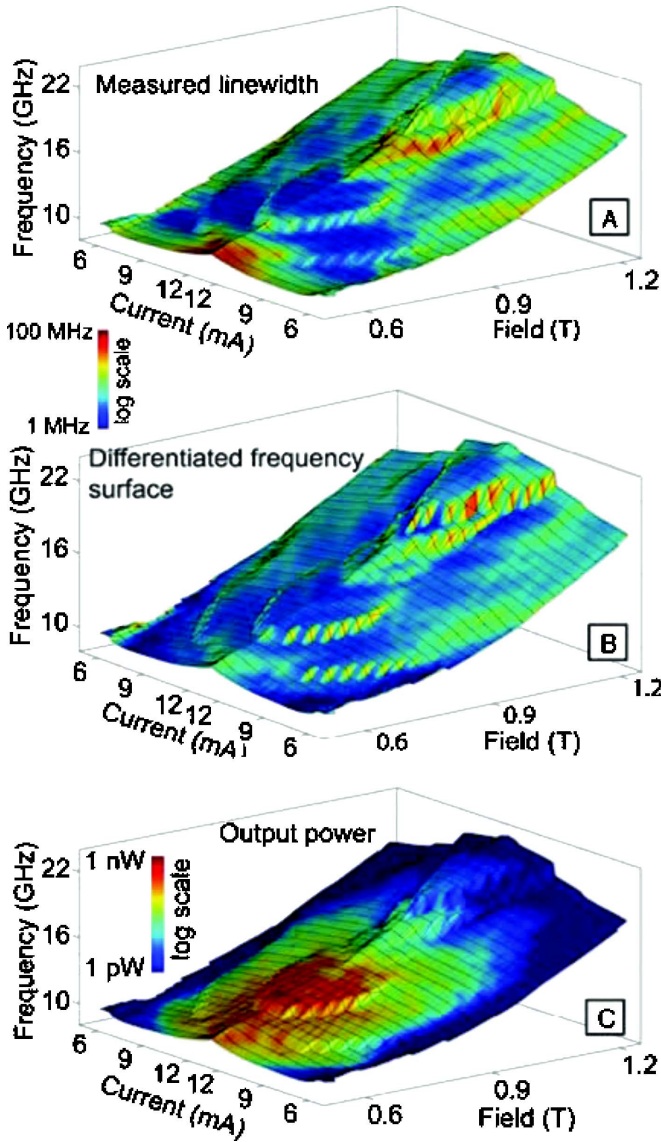


FIG. 3. (Color online) (A)–(C) Plots showing (A) the measured linewidth (FWHM), (B) the magnitude of the numerical differentiation of the frequency surface through Eq. (1), and (C) the device output power for  $\theta_H=80^\circ$  mapped onto the corresponding frequency surface [Fig. 1(e)]. The color scale for (A) and (B) is logarithmic and ranges from 1 to 100 MHz.

high measured linewidths and regions having large calculated linewidths. The correlation is particularly strong when there is a discontinuous jump in the oscillation frequency in either current or applied field, where the gradient of the frequency surface is strongest. Similarly, a strong correlation occurs between regions having measured linewidths on the order of a few MHz, and regions having narrow linewidths in the calculation. This indicates that the narrowest linewidths we have measured in the nanocontact devices may be limited by instrumentation noise rather than reflecting the intrinsic oscillator linewidths. We note that quantitative comparison between the differentiated surface and the measured linewidth cannot be made at the discontinuous jumps, because the frequency surface is not strictly differentiable at these locations and must be numerically smoothed. Furthermore, at

the discontinuities linewidth broadening due to the finite dwell-time effects also must be taken into account, which is not included in this model.

Similar comparisons between the measured linewidths and those predicted by Eq. (1) for other field angles give significantly worse agreement. For example, for the  $\theta_H=50^\circ$  surface, the average  $df/dI_{dc}$  is smaller than for the  $\theta_H=80^\circ$  surface and  $df/dH$  is roughly 50% larger than for  $\theta_H=80^\circ$ . Eq. (1) would predict that the average linewidth for the  $\theta_H=50^\circ$  data is only slightly larger than for  $\theta_H=80^\circ$ , assuming the same values for  $\Delta H$  and  $\Delta I_{dc}$ . Instead, the measured linewidths for  $\theta_H=50^\circ$  are roughly a factor of five larger than for  $\theta_H=80^\circ$ . This discrepancy would remain even if other sources of thermal noise were included in the model, assuming that the other sources would contribute equally for all applied field angles. This shows that the linewidth cannot generally be attributed to a constant thermal noise source, but may be limiting the narrowest peaks that we measure.

There are also correlations between the device output power (integrated area under a spectral peak) and discontinuous changes in the frequency surface, as shown in Fig. 3(c). For instance, for  $\mu H=0.7$  T and  $I_{dc}=11$  mA the output power changes by a factor of 2 across the frequency discontinuity. The increase in power is not simply associated with the increase in current since a similar increase is not found at higher field values, and the power output increases abruptly at the frequency jumps. As was discussed above, this is consistent with a significant change in the precessional trajectories, i.e., the oscillation mode structure, occurring at these locations. However, there is not always a significant change in power output at a frequency jump, as seen at the highest applied field values. We note that the fine structure in the measured linewidth within a given plateau results, at least primarily, from standing-wave resonances in the measurement circuit.

As shown by the data for  $\theta_H=50^\circ$  in Fig. 4(a), frequency surfaces that are nominally planar in field and current can also yield complicated and nonmonotonic linewidth surfaces. For instance, for  $\mu H=0.65$  T the frequency surface is nominally planar while the linewidth varies from greater than 1 GHz to less than 100 MHz for  $I_{dc}$  ranging from 8 to 10 mA. Furthermore, even the qualitative evolution of the linewidth with current changes as a function of applied field strength. At low applied fields the linewidth is relatively large at onset, then decreases, before increasing again at higher currents, whereas the opposite behavior occurs at the highest applied field [Fig. 4(b)]. This is one example of the complexity of the precessional dynamics induced by the spin-transfer effect and leads to questions regarding the utility of comparing experimental work to theoretical predictions over only a small range of applied fields, currents, and geometries.

In order to more quantitatively summarize the variation of output power we plot the average output power as a function of the applied field strength for various field angles in Fig. 5. The data represent the average output power over the swept current range for a particular applied field strength and angle. For moderate applied field strengths the maximum device output power occurs for fields applied nearly out of plane. As seen in the figure, the maximum output power occurs for

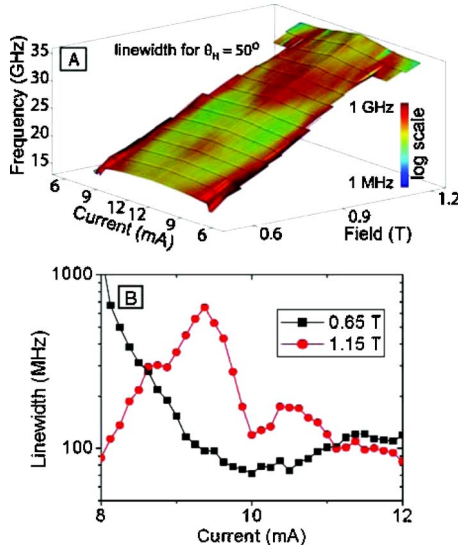


FIG. 4. (Color online) (A) Plot showing the measured linewidth (FWHM) for  $\theta_H=50^\circ$  mapped onto the corresponding frequency surface [Fig. 1(a)]. The color scale is logarithmic and ranges from 1 MHz to 1 GHz. (b) Plots explicitly showing the measured linewidth for  $\mu_0 H=0.65$  and 1.15 T in part (A).

$\theta_H \approx 80^\circ$  and  $\mu_0 H \approx 0.7$  T to 0.8 T, as is generally the case for devices with CoFe and NiFe as the fixed and free layers, respectively. The field value at which the maximum occurs increases with angle. For all directions of the applied field, the device output power decreases to small values at the largest applied field values. This is consistent with the device power output resulting from the GMR effect, which depends on the relative angle between the magnetization directions of the two layers. For large applied fields, the relative angle between the layers should be the smallest.

In Fig. 6(a) we show the average oscillation linewidth for the frequency surfaces shown in Fig. 1 along with their median values. While there is significant variation in the linewidth for any applied field direction, on average the linewidth decreases with increasing applied field angle and reaches its smallest value for  $\theta_H=80^\circ$  before increasing again at  $\theta_H=85^\circ$ . The averaging includes locations where the oscillator has particularly large linewidths, e.g., at the fre-

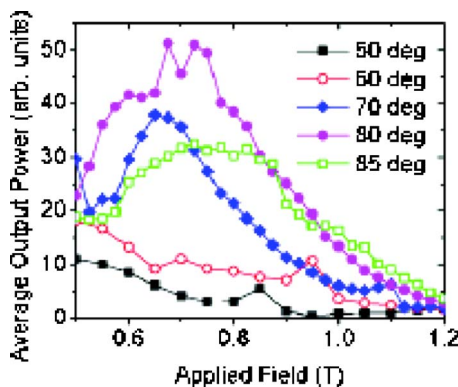


FIG. 5. (Color online) Plot showing the device output power versus the applied field for the frequency surfaces shown in Fig. 1. The power is averaged over the current sweep.

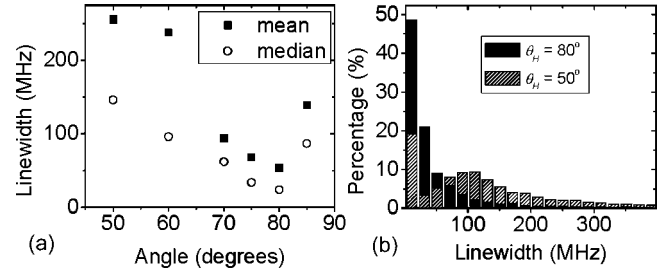


FIG. 6. (a) Plot showing the mean and median values of the measured linewidth as a function of the applied field angle. The values are determined by averaging the linewidths over the entire frequency surfaces shown in Fig. 1. (b) Histogram of the measured linewidths over the entire frequency surfaces for applied field angles of  $50^\circ$  and  $80^\circ$ . The bin size is 20 MHz.

quency discontinuities, and these large values skew the average for a given field geometry. This somewhat deemphasizes the narrowness of the oscillation linewidths over much of the various surfaces, as can be seen by comparing the mean and median linewidth values. A comparison of the distribution of linewidths at the lowest and highest field angles is shown more explicitly by the histograms in Fig. 6(b). For  $\theta_H=50^\circ$  the distribution is bimodal consisting of roughly 20% of the oscillator linewidths being less than 20 MHz and the mean of the distribution being roughly 250 MHz. In comparison, for  $\theta_H=80^\circ$ , approximately 50% of linewidths are less than 20 MHz and the mean of the distribution is approximately 50 MHz.

As can be seen in Fig. 3 the oscillator linewidths can be as small as a few MHz over much of the surfaces for large angles of  $\theta_H$ . It has been suggested that narrow linewidths in spin-transfer oscillators may result from a localization of the excited mode in these structures.<sup>35</sup> However, here we show that the narrowest linewidths occur for an applied field direction that is nearly out of plane. Elsewhere,<sup>36</sup> we have explicitly shown that in this geometry the mode is not localized but leads to propagation of spin waves into the surrounding film, demonstrating that localization is not responsible for the narrowness of the measured linewidths.

The cause of the overall trend of the excitation linewidth with applied field angle is not presently clear. FMR measurements have shown that as the magnetization is rotated into the out-of-plane direction, the number of degenerate spin-wave modes decreases, thus decreasing the two-magnon damping rate and the FMR linewidth.<sup>37,38</sup> This mechanism could also be responsible for the similar decrease in linewidth measured here. Another possibility is that the narrower linewidths at higher angles results from the oscillations being of the largest amplitude at these field geometries, as has been suggested for nanopillar devices.<sup>39</sup> This is possibly supported by the correlation between the oscillators generally having the narrowest linewidths and largest output powers for roughly  $\theta_H=80^\circ$ . However, because the device output results from the GMR effect one generally expects an increase in the output power as the applied field angle is increased, independent of the precessional angle.<sup>31</sup> Furthermore, as shown at the highest applied field values in Fig. 3, regions of narrow linewidths are not exclusive to high output power, large-

angle precession, indicating that other effects must also be taken into account. Because of the discrepancies between the single-domain model and the measured response of the nanocontact devices, as discussed above, we do not find it meaningful to compare the measured linewidth and the linewidth predicted by the single-domain model.

In summary, we have measured the precessional dynamics in spin-transfer nanocontact devices for a range of applied field strengths and angles. The excited frequencies qualitatively agree with those predicted from the single-domain model. However, the details of the evolution of the frequency with current and field at high angles of applied field differ from the predicted behavior. In particular, the frequency undergoes discontinuous jumps with both current and applied field. These jumps appear to be associated with changes in

the mode structure, i.e., precessional trajectories, of the free-layer magnetization that can also result in significant changes in the oscillator linewidth and output power. While the particular locations of these discontinuities vary from device to device, we have found their existence robust with respect to contact size, field strength, free-layer material, and devices fabricated by different groups.<sup>13</sup> There are correlations between the discontinuities in the frequency evolution and the device output power and the spectral linewidth. Combined, these create a complex spectral signature, particularly at high applied field angles, that is not well simulated using either single-domain or micromagnetic modeling. The data presented are intended to provide a set of measurements to which future theory and measurement can be compared.

- 
- <sup>1</sup>J. C. Slonczewski, *J. Magn. Magn. Mater.* **159**, L1 (1996); **195**, L261 (1999).
- <sup>2</sup>L. Berger, *Phys. Rev. B* **54**, 9353 (1996).
- <sup>3</sup>J. A. Katine, F. J. Albert, R. A. Buhrman, E. B. Myers, and D. C. Ralph, *Phys. Rev. Lett.* **84**, 3149 (2000).
- <sup>4</sup>S. Urazhdin, N. O. Birge, W. P. Pratt, and J. Bass, *Phys. Rev. Lett.* **91**, 146803 (2003).
- <sup>5</sup>T. Devolder, P. Crozat, C. Chappert, J. Miltat, A. Tulapurkar, Y. Suzuki, and K. Yagami, *Phys. Rev. B* **71**, 184401 (2005).
- <sup>6</sup>J. Grollier, V. Cros, A. Hamzic, J. M. George, H. Jaffrès, A. Fert, G. Faini, J. Ben Youssef, and H. Legall, *Appl. Phys. Lett.* **78**, 3663 (2001).
- <sup>7</sup>B. Özyilmaz, A. D. Kent, D. Monsma, J. Z. Sun, M. J. Rooks, and R. H. Koch, *Phys. Rev. Lett.* **91**, 067203 (2003).
- <sup>8</sup>D. Chiba, Y. Sato, T. Kita, F. Matsukura, and H. Ohno, *Phys. Rev. Lett.* **93**, 216602 (2004).
- <sup>9</sup>F. B. Mancoff, R. W. Dave, N. D. Rizzo, T. C. Eschrich, B. N. Engel, and S. Tehrani, *Appl. Phys. Lett.* **83**, 1596 (2003).
- <sup>10</sup>J. E. Wegrowe, A. Fabian, Ph. Guittienne, X. Hoffer, D. Kelly, J.-Ph. Ansermet, and E. Olive, *Appl. Phys. Lett.* **80**, 3775 (2002).
- <sup>11</sup>M. Tsoi, A. G. M. Jansen, J. Bass, W. C. Chiang, M. Seck, V. Tsoi, and P. Wyder, *Phys. Rev. Lett.* **80**, 4281 (1998).
- <sup>12</sup>W. H. Rippard, M. R. Pufall, S. Kaka, S. E. Russek, and T. J. Silva, *Phys. Rev. Lett.* **92**, 027201 (2004).
- <sup>13</sup>F. B. Mancoff, N. D. Rizzo, B. N. Engel, and S. Tehrani, *Appl. Phys. Lett.* **88**, 112507 (2006).
- <sup>14</sup>T. Y. Chen, Y. Ji, and C. L. Chien, *Appl. Phys. Lett.* **84**, 380 (2004).
- <sup>15</sup>A. Yamaguchi, T. Ono, S. Nasu, K. Miyake, K. Mibu, and T. Shinjo, *Phys. Rev. Lett.* **92**, 077205 (2004).
- <sup>16</sup>A. Slavin and V. Tiberkevich, *Phys. Rev. Lett.* **95**, 237201 (2005).
- <sup>17</sup>G. Bertotti, C. Serpico, I. D. Mayergoyz, A. Magni, M. d'Aquino, and R. Bonin, *Phys. Rev. Lett.* **94**, 127206 (2005).
- <sup>18</sup>N. Smith, cond-mat/0406486 (unpublished).
- <sup>19</sup>M. A. Hoefer, M. J. Ablowitz, B. Ilan, M. R. Pufall, and T. J. Silva, *Phys. Rev. Lett.* **95**, 267206 (2005).
- <sup>20</sup>M. D. Stiles and A. Zangwill, *Phys. Rev. B* **66**, 014407 (2002).
- <sup>21</sup>S. M. Rezende, F. M. de Aguiar, and A. Azevedo, *Phys. Rev. B* **73**, 094402 (2006).
- <sup>22</sup>Ya. B. Bazsaliy, B. A. Jones, and S. C. Zhang, *Phys. Rev. B* **69**, 094421 (2004).
- <sup>23</sup>X. Waintal and O. Parcollet, *Phys. Rev. Lett.* **94**, 247206 (2005).
- <sup>24</sup>S. E. Russek, S. Kaka, W. H. Rippard, M. R. Pufall, and T. J. Silva, *Phys. Rev. B* **71**, 104425 (2005).
- <sup>25</sup>J. Z. Sun, *Phys. Rev. B* **62**, 570 (2000).
- <sup>26</sup>J. Xiao, A. Zangwill, and M. D. Stiles, *Phys. Rev. B* **72**, 014446 (2005).
- <sup>27</sup>K.-J. Lee, A. Deac, O. Redon, J.-P. Nozieres, and B. Dieny, *Nat. Mater.* **3**, 877 (2004).
- <sup>28</sup>B. Montigny and J. Miltat, *J. Appl. Phys.* **97**, 10C708 (2005).
- <sup>29</sup>D. V. Berkov and N. L. Gorn, *J. Appl. Phys.* **99**, 08Q701 (2006).
- <sup>30</sup>See, for instance, M. D. Stiles and J. Miltat, in *Spin Dynamics in Confined Magnetic Structures III*, edited by B. Hillebrands and A. Thiaville (Springer, Berlin, 2005) for a comprehensive review.
- <sup>31</sup>W. H. Rippard, M. R. Pufall, S. Kaka, T. J. Silva, and S. E. Russek, *Phys. Rev. B* **70**, 100406(R) (2004).
- <sup>32</sup>W. H. Rippard, M. R. Pufall, S. Kaka, T. J. Silva, S. E. Russek, and J. A. Katine, *Phys. Rev. Lett.* **95**, 067203 (2005).
- <sup>33</sup>S. I. Kiselev, J. C. Sankey, I. N. Krivorotov, N. C. Emley, R. J. Schoelkopf, R. A. Buhrman, and D. C. Ralph, *Nature (London)* **425**, 308 (2003).
- <sup>34</sup>J. C. Sankey, P. M. Braganca, A. G. F. Garcia, I. N. Krivorotov, R. A. Buhrman, and D. C. Ralph, *Phys. Rev. Lett.* **96**, 227601 (2006).
- <sup>35</sup>Q. Mistral, J.-K. Kim, T. Devolder, P. Crozat, C. Chappert, J. A. Katine, M. J. Carey, and K. Ito, *Appl. Phys. Lett.* **88**, 192507 (2006).
- <sup>36</sup>M. R. Pufall, W. H. Rippard, S. E. Russek, S. Kaka, and J. A. Katine, *Phys. Rev. Lett.* **97**, 087206 (2006).
- <sup>37</sup>R. D. McMichael, M. D. Stiles, P. J. Chen, and W. F. Egelhoff, Jr., *J. Appl. Phys.* **83**, 7037 (1998).
- <sup>38</sup>M. J. Hurben and C. E. Patton, *J. Appl. Phys.* **83**, 4344 (1998).
- <sup>39</sup>J.-V. Kim, *Phys. Rev. B* **73**, 174412 (2006).